

## THE THREE-DIMENSIONAL STRUCTURE OF A RADIATIVE, COSMIC BULLET FLOW

A. C. RAGA,<sup>1</sup> A. ESQUIVEL,<sup>1</sup> A. RIERA,<sup>2,3</sup> AND P. F. VELÁZQUEZ<sup>1</sup>

Received 2007 May 9; accepted 2007 June 25

### ABSTRACT

We have carried out an axisymmetric and a three-dimensional (3D) numerical simulation of a radiative, interstellar bullet flow with the same physical and numerical setup. We find that while some of the main features of the axisymmetric flow are reproduced in the 3D simulation (e.g., the production of “vortex shedding events” and the fragmentation of the head of the bullet flow), strong deviations from axisymmetry occur in the 3D flow. The main difference between the axisymmetric and the 3D flows is that the on-axis, high-velocity condensation that is characteristic of the axisymmetric flow does not appear in the 3D bullet flow.

*Subject headings:* ISM: Herbig-Haro objects — ISM: jets and outflows — ISM: kinematics and dynamics — planetary nebulae: general

### 1. INTRODUCTION

Radiative, “interstellar bullet” flows (in which a high-density condensation propagates in a diffuse medium) have been proposed for modeling HH objects (Norman & Silk 1979). “Bullet” models have been present from the very beginning of dynamical modeling of HH objects (Hartmann & Raymond 1984), and are still present in different guises in the more recent literature.

Also, observations of planetary nebulae (PNe) reveal the existence of clumps in a number of objects. Those clumps usually show low-excitation spectra, and are dense and molecular. Some clumps show a cometary tail morphology when observed at the high angular resolution provided by the *Hubble Space Telescope* (such as the striking cometary tails of the neutral globules in NGC 7293; see, e.g., O’Dell et al. 2002).

Knots and/or filaments with low-excitation spectra and moving at velocities larger than the expansion velocity of the shell are found in several PNe (see, e.g., Corradi et al. 1999; Gonçalves et al. 2004). Several objects show pairs of symmetrically opposed knots (in some cases with bow-shaped morphologies), which strongly suggest the occurrence of episodic ejections from the central star. In such systems, the bow-shock-like knots resemble the structure formed as a high-velocity “bullet” moves through the environmental material, as first proposed by Poludnenko et al. (2004a). The cosmic bullet scenario in such objects is reinforced by the presence of Hubble-type flows (i.e., velocities increasing linearly with distance to the source), which is the predicted behavior in the wake of a bullet (Poludnenko et al. 2004a).

The “cosmic bullet” flow is also applicable for high-density clumps forming part of supernova remnants. An example of this are the high-velocity clumps found in the ejecta associated with the young remnant Cassiopeia A (Fesen et al. 2006). Also, basically the same flow configuration is relevant for the case of a SN remnant overrunning clumps present in the surrounding medium (a dramatic example of this appears to be the very young SN 1987A remnant; see, e.g., Bouchet et al. 2006).

Numerical simulations of axisymmetric, radiative bullet flows have been carried out by Raga et al. (1998) and by Poludnenko et al. (2004b). Raga et al. (1998) simulated an initially stationary bullet which is overrun by an impinging, plane-parallel flow. Poludnenko et al. (2004b) simulated a high-velocity bullet moving with respect to a stationary environment, and followed the bullet to larger evolutionary times. Both of these papers show that the axisymmetric, radiative bullet flow has a number of “vortex shedding” events, and that it produces a high-density, on-axis condensation that preserves a high velocity (with respect to the surrounding medium) throughout the evolution of the flow.

In the present paper we address the question of whether or not the main features of the axisymmetric flow are maintained in a three-dimensional (3D) simulation, or whether the 3D flow deviates in a drastic way from the axisymmetric flow. This question has been addressed to some extent by Klein et al. (2003) for the case of a nonradiative bullet flow. These authors show one graph of the density distribution obtained from a 3D simulation, illustrating the fact that strong deviations from axisymmetry do occur. Xu & Stone (1995) present a much more detailed study, in which they quantify the global properties of a 3D bullet flow.

Also relevant in the context of the present work are the papers of Gregori et al. (2000), who present 3D simulations of magnetized bullet flows. Also, Falle et al. (2002), compute axisymmetric simulations including the “K- $\epsilon$ ” turbulence parameterization. This work is particularly interesting as it explores the effects of introducing parameterized turbulence models into astrophysical bullet flow simulations.

We have computed an axisymmetric and a 3D simulation of a radiative, interstellar bullet flow with the same parameters, and numerical and physical setup. Both the parameters and the resolution are similar to the ones of the simulation of Poludnenko et al. (2004b). We then compare the time-evolution of the axisymmetric and 3D flows in order to evaluate how large are the deviations between the two flows.

We describe the numerical and physical model in § 2. The results from the simulations are shown in § 3. Finally, a qualitative discussion of the results is given in § 4.

### 2. THE NUMERICAL SIMULATIONS

We have carried out an axisymmetric and a 3D (Cartesian) numerical simulation with almost identical initial and boundary conditions. We have considered an initially spherical bullet with a

<sup>1</sup> Instituto de Ciencias Nucleares, Universidad Nacional Autónoma de México, 04510 D.F., México.

<sup>2</sup> Departament de Física i Enginyeria Nuclear, Escola Universitària d’Enginyeria Tècnica Industrial de Barcelona, Universitat Politècnica de Catalunya, 08036 Barcelona, Spain.

<sup>3</sup> Departament d’Astronomia i Meteorologia, Universitat de Barcelona, E-08028 Barcelona, Spain.

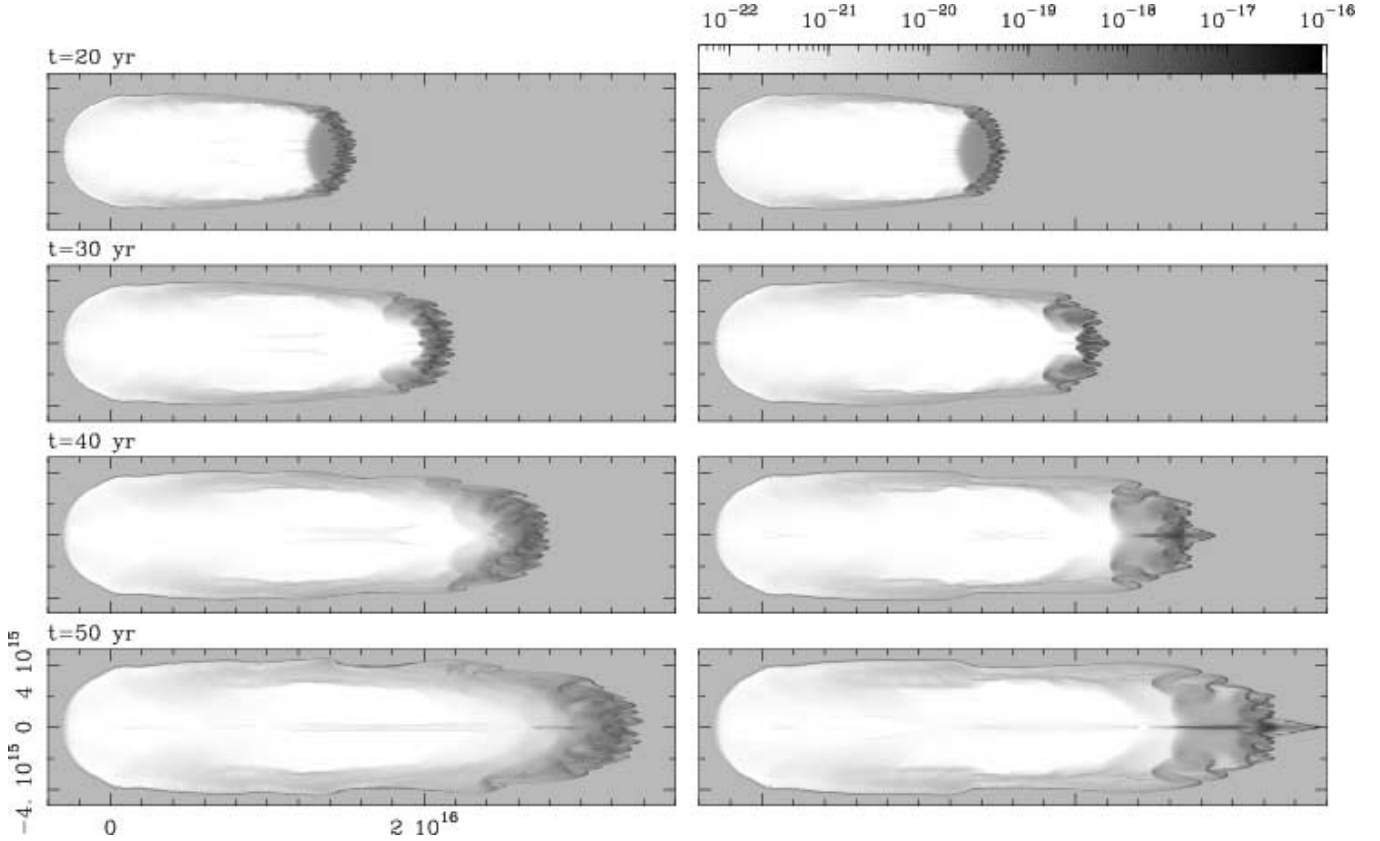


FIG. 1.—Density stratifications on the  $(x, y)$ -plane of the 3D simulation (*left*) and on the  $(x, r)$ -plane of the axisymmetric simulation (*right*, with the bottom half of the plots corresponding to a reflection on the symmetry axis of the computed flow structure) for four different integration times. The integration times are shown (in years) on top of each of the plots on the left. The density stratifications are depicted with the logarithmic gray scale shown (with densities in  $\text{g cm}^{-3}$ ) by the bar on the top right. The axes are given in cm, with  $(x, y) = (0, 0)$  corresponding to the central position of the initial clump.

$r_b = 3 \times 10^{15}$  cm radius which is moving along the  $x$ -axis of the domain at a  $v_b = 250 \text{ km s}^{-1}$  velocity within an initially homogeneous, stationary medium of number density  $n_a = 10^4 \text{ cm}^{-3}$  and temperature  $T_a = 100 \text{ K}$ .

The bullet has an initial temperature  $T_b = 10 \text{ K}$  and in the axisymmetric simulation has a uniform,  $n_b = 10^5 \text{ cm}^{-3}$  number density. In the 3D simulation, we choose a sinusoidally perturbed initial density for the bullet given by

$$n_b(x, y, z) = n_0 \left\{ 1 + \frac{0.05}{3} \left[ \sin\left(\frac{2\pi x}{l_0}\right) + \sin\left(\frac{2\pi y}{l_0}\right) + \sin\left(\frac{2\pi z}{l_0}\right) \right] \right\}, \quad (1)$$

with  $n_0 = 10^5 \text{ cm}^{-3}$ ,  $l_0 = 10^{15}$  cm. The  $(x, y, z)$  coordinate system is centered on the initial position of the bullet. In other words, the bullet in the 3D numerical simulation has basically the same density as the one of the axisymmetric simulation, but with a 3D sinusoidal perturbation with a wavelength of one-third of the initial bullet radius and peak deviations of  $\pm 5\%$ .

The simulations are carried out with 2D and 3D versions of the *guazu*—a code. This code integrates the gasdynamic equations together with a set of atomic/ionic/chemical rate equations in a binary, adaptive grid. The code is described in detail by Raga et al. (2000), and the present calculations were carried out solving only a single rate equation for the ionization of H and using the parameterized cooling function (calculated as a function of the tem-

perature, density and neutral fraction) of Raga et al. (1999). A seed electron density of  $10^{-4}$  times the total number density was assumed for the initially neutral bullet and environmental material.

The axisymmetric simulation was carried out in a computational domain with a radial extent of  $5 \times 10^{15}$  cm and an axial extent of  $4 \times 10^{16}$  cm (extending from  $x = -4 \times 10^{15}$  cm to  $x = 3.6 \times 10^{16}$  cm, with  $x = 0$  corresponding to the initial position of the center of the bullet). A reflection condition was applied on the symmetry axis, and an outflow condition was applied on all of the other grid boundaries.

The 3D simulation was carried out in a Cartesian grid extending  $(4, 1, 1) \times 10^{16}$  cm along the  $(x, y, z)$  direction axes. An outflow condition was applied on all of the grid boundaries.

Both simulations were carried out on a six-level binary adaptive grid, with a maximum resolution of  $3.9 \times 10^{13}$  cm along all axes (this resolution would correspond to a  $1024 \times 128$  axisymmetric and a  $1024 \times 256 \times 256$  3D, uniform grid simulation). We label the bullet material with a passive scalar, and then require the regions with the identified clump material to be refined at least to the fourth grid level, which has a resolution of  $1.56 \times 10^{14}$  cm. This requirement ensures an appropriate numerical resolution of the initial, low-amplitude density perturbation of the bullet in the 3D simulation (see eq. [1]).

At the highest resolution of the adaptive grid, the initial bullet radius is resolved with  $\approx 76$  grid points. This resolution is somewhat lower than the one of the axisymmetric simulation of Poludnenko et al. (2004b), who resolved the initial bullet radius with 128 grid points, and similar to the one of the 3D, nonradiative simulation

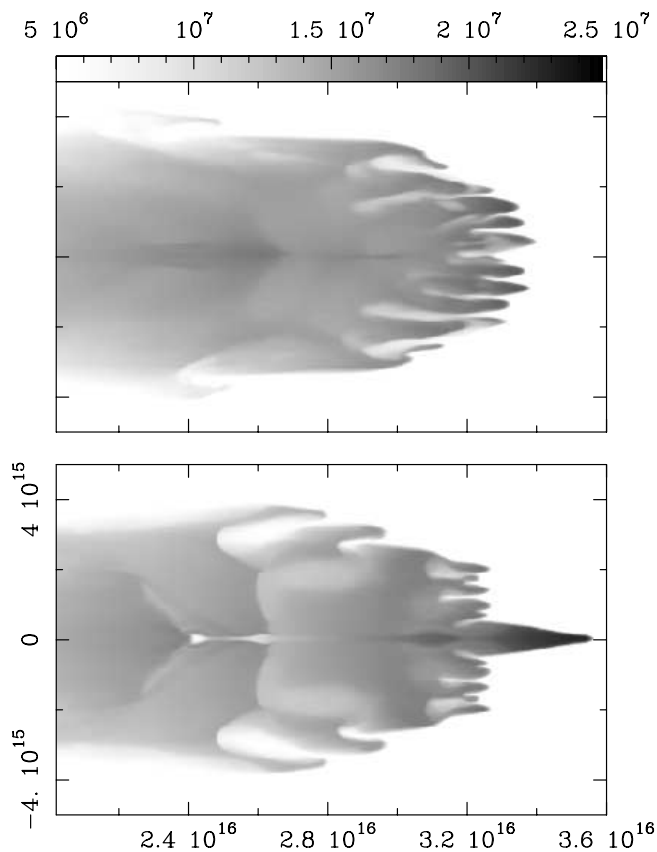


FIG. 2.—Stratification on the  $(x, y)$ -plane (*top*) and  $(x, r)$ -plane (*bottom*) of the velocity along the flow axis ( $v_x$ ) obtained for a  $t = 50$  yr time integration from the 3D (*top*) and axisymmetric (*bottom*) simulations. Only part of the computational domain is shown (see Fig. 1). The velocity stratification is shown with the linear scale given (in  $\text{cm s}^{-1}$ ) by the top bar. The axes are labeled in cm, and the stratification obtained from the axisymmetric simulation (*bottom*) has been reflected on the symmetry axis.

of Klein et al. (2003, who resolved the initial bullet radius with 90 grid points). In the “high-resolution” simulation of Xu & Stone (1995), the initial bullet radius is resolved with 53 points.

We should note that the parameters of our simulations are very similar to the ones of the bullet model of Poludnenko et al. (2004b), except for the fact that our ambient medium is 10 times denser. We have chosen a higher density environment for the following reason.

The motion of a bullet of density  $n_b$ , moving at a velocity  $v_b$  through a medium of density  $n_a$  induces a “cloudlet shock” (within the body of the bullet) of velocity  $v_{cs} \approx v_b$ . This cloudlet shock travels through the diameter of the bullet in a time

$$t_c = \frac{2r_b}{v_{cs}} \approx \frac{2r_b}{v_b} \sqrt{\frac{n_b}{n_a}}. \quad (2)$$

After the passage of the cloudlet shock, the compressed bullet suffers a strong fragmentation.

Poludnenko et al. (2004b) give a somewhat more complex estimate for  $t_c$  (which actually gives very similar results to the ones of eq. [2]), and call it the “clump crushing time.” The simulation of Poludnenko et al. (2004b) had a  $t_c = 81$  yr clump crushing time (see eq. [2]), and the evolution of the clump material was followed until a time  $t_f = 250$  yr  $\approx 3t_c$ . In order to follow this evolution, they needed a computational grid with an axial extent of  $D \approx t_f v_b = 1.8 \times 10^{17}$  cm.

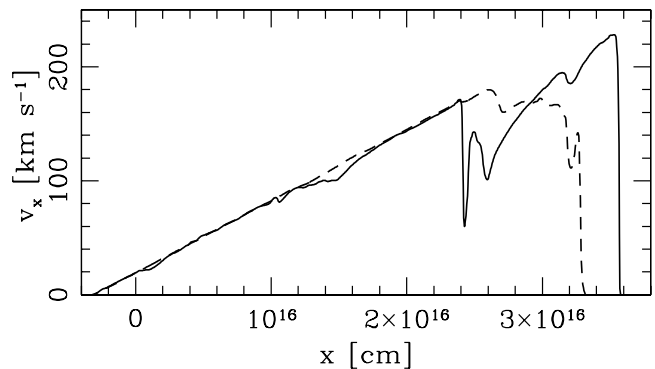


FIG. 3.—Cuts along the  $x$ -axis of the  $x$ -component  $v_x$  of the flow velocity obtained from the  $t = 50$  yr frame of the axisymmetric (*solid line*) and the 3D (*dashed line*) simulations.

The parameters of our simulations are very similar to the ones of Poludnenko et al. (2004b), except for the fact that we have a 10 times higher ambient density. With our parameters, we obtain  $t_c = 24$  yr. Then, in a grid with an axial extent of only  $D = 4 \times 10^{16}$  cm we can follow the time evolution of the clump up to a time  $t_f \approx D/v_b \approx 50$  yr, approximately 2 times the cloud crushing timescale  $t_c$ .

Finally, let us discuss the dimensionless parameters associated with our simulation. The simulation has an initial clump to environment density ratio of  $\approx 10$ , and pressure ratio of  $\approx 1$  (the 3D simulation having only low-amplitude density and pressure perturbations; see eq. [1]). The bullet material has an initial Mach number of 766 with respect to the bullet sound speed, and of 242 with respect to the environmental sound speed, so that it is therefore well into the high Mach number, “strong shock” regime.

In the on-axis region, the bow shock has a shock velocity of  $\approx 190$   $\text{km s}^{-1}$ , and the cloudlet shock has a shock velocity of  $\approx 60$   $\text{km s}^{-1}$ . Using these shock velocities and the corresponding preshock densities, by an appropriate scaling of the models of Hartigan et al. (1987), one obtains a cooling distance (to  $10^4$  K)  $d_{bs} \approx 1.7 \times 10^{12}$   $\text{cm}^{-3}$  and  $d_{cs} \approx 1.8 \times 10^{10}$   $\text{cm}^{-3}$  for the bow shock and the cloudlet shock, respectively, corresponding to cooling distance to initial bullet radius ratios of  $d_{bs}/r_c = 5.7 \times 10^{-4}$  and  $d_{cs}/r_c = 6.0 \times 10^{-6}$ . We should note that these cooling distances are hopelessly unresolved in our simulations, but that this is a necessary flaw if we want to have parameters comparable to the ones of Poludnenko et al. (2004b).

We have then carried out the axisymmetric and 3D numerical simulations described above, stopping the simulations when the bullet material starts to leave the computational domain. The results of the simulations are described in the following section.

### 3. THE AXISYMMETRIC AND THE 3D BULLET FLOWS

Figure 1 shows a time sequence of the density stratification on the  $(x, y)$ -plane (cutting through the center of the bullet) for the 3D simulation, and on the  $(x, r)$ -plane for the axisymmetric simulation. The bullet is initially centered on the origin of the coordinate system, and propagates to the right (along the  $x$ -axis) as a function of increasing time.

At early times (see the  $t = 20$  yr frame of Fig. 1), the density stratifications of the 3D and axisymmetric simulations are most similar, and the deviations from axisymmetry (of the 3D bullet) can only be seen by looking at the details of the leading region of the bow shock.

In the  $t = 30$  yr frame (see Fig. 1), a first “vortex shedding event” has occurred in both simulations. This first vortex lags

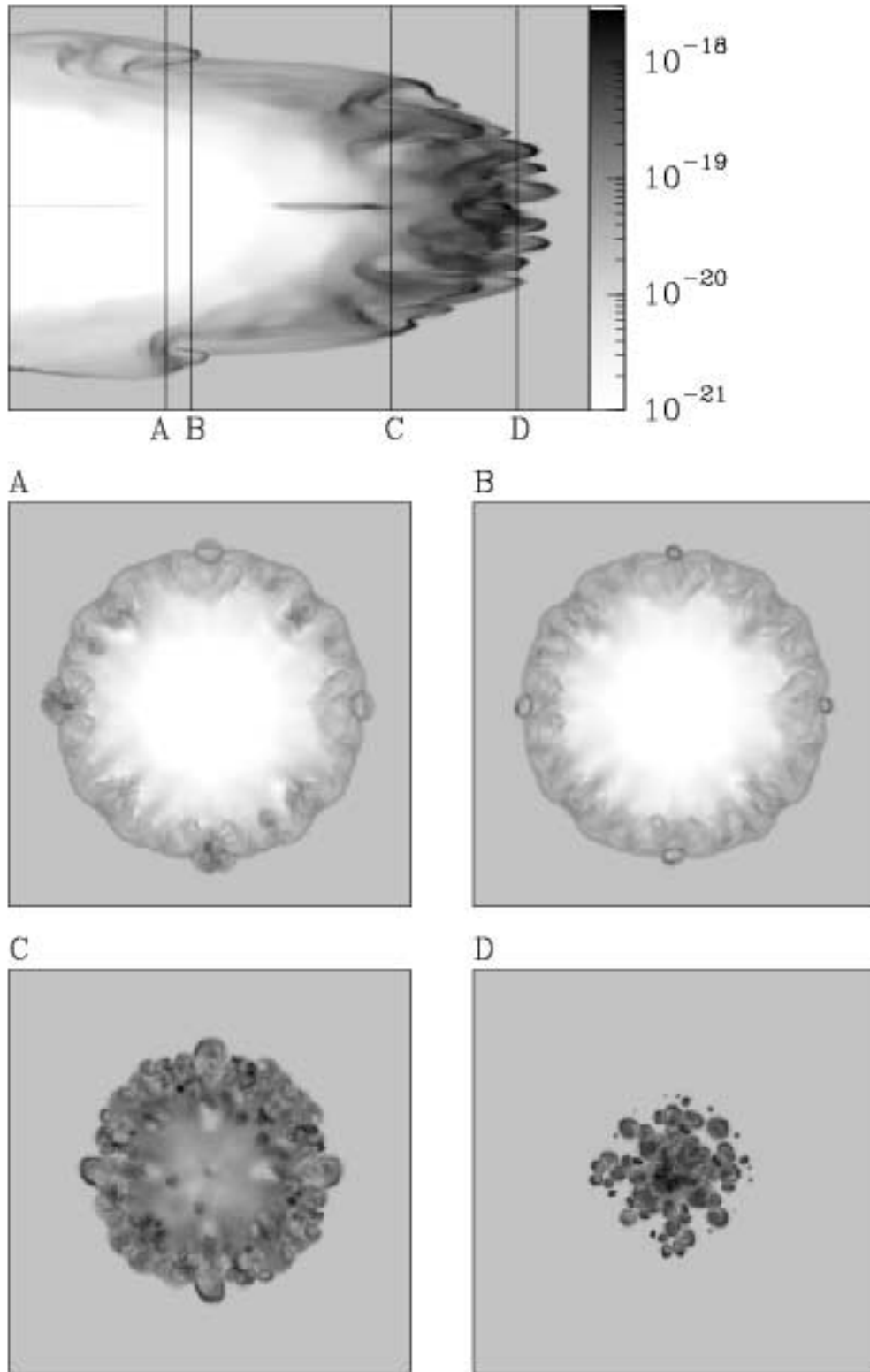


FIG. 4.—Density stratification obtained from the 3D simulation for a  $t = 50$  yr integration time. The top graph shows an  $(x, y)$ -cut (i.e., at  $z = 0$ ) of the region with  $2.02 \times 10^{16}$  cm  $< x < 3.47 \times 10^{16}$  cm and  $-5.0 \times 10^{15}$  cm  $< y < 5.0 \times 10^{15}$  cm. On this plot, we show the position of four cuts parallel to the  $y$ - $z$  plane, at positions  $x = 2.41 \times 10^{16}$  cm (cut A),  $x = 2.48 \times 10^{16}$  cm (cut B),  $x = 2.98 \times 10^{16}$  cm (cut C), and  $x = 3.29 \times 10^{16}$  cm (cut D). The density stratifications in these cross-flow axis cuts are shown in the four bottom plots (which include the full  $y$ - $z$  extent of the computational domain). The density stratifications are shown with the logarithmic gray scale given by the bar on the right of the top plot (in  $\text{g cm}^{-3}$ ).

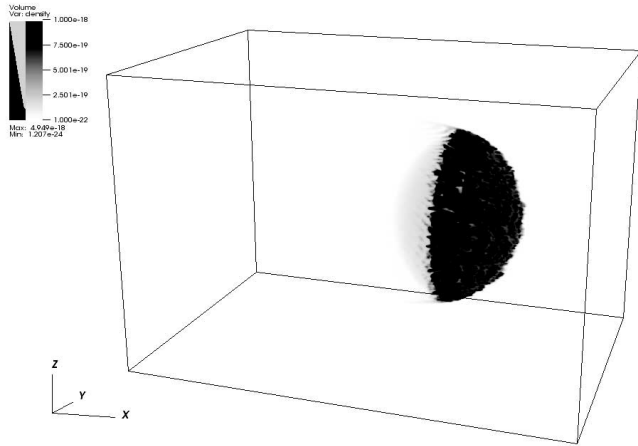


FIG. 5.—Volume-rendered representation of the density stratification obtained from the 3D simulation for a  $t = 10$  yr time integration. Only part of the  $x$ -extent of the computational domain is shown. The bar on the top left shows the linear gray scale (in units of  $\text{g cm}^{-3}$ ) and the “transparency” scale.

behind the main bullet flow and has a substantially slower motion in the 3D than in the axisymmetric simulation. In the  $t = 50$  yr frame, this first vortex has reached  $x \approx 2.8 \times 10^{16}$  cm in the axisymmetric model, but has reached only  $x \approx 2.5 \times 10^{16}$  cm in the 3D simulation. The axisymmetric simulation sheds a second vortex (seen in the  $t = 40$  yr frame of Fig. 1), and is starting to produce a third vortex at  $t = 50$  yr. The 3D simulation is only starting to produce a second vortex at  $t = 50$  yr.

One of the important features of the axisymmetric simulation is the production of a leading, on-axis, compact clump at the head of the bow shock. In Figure 2 (which shows the axial velocity stratification at  $t = 50$  yr), we see that this axial clump has a  $v = 228 \text{ km s}^{-1}$  velocity, which is very close to the initial velocity of the bullet flow.

Such an axial clump is not produced in the 3D simulation. The leading bow shock shows a number of off-axis protrusions (see Fig. 1), which have velocities of  $\approx 195 \text{ km s}^{-1}$  (see Fig. 2). These structures resemble (both in morphology and axial velocity) the off-axis structures of the axisymmetric simulation.

A kinematic property of the axisymmetric simulations of radiative cosmic bullets is the presence of a Hubble-type flow in the bullet wake (see, e.g., Poludnenko et al. 2004b). Figure 3 shows cuts along the  $x$ -axis of the  $x$ -component  $v_x$  of the flow velocity obtained from the 3D and axisymmetric simulations (for  $t = 50$  yr). Both stratifications show a linear increase of the velocity with distance (where  $x = 0$  corresponds to the central position of the initial clump) up to  $x \approx 2.4 \times 10^{16}$  cm with similar slopes. Strong deviations between both simulations occur at larger  $x$  values, close to the head of the bullet flow.

Let us now discuss in more detail the deviations from axisymmetry that occur in the 3D simulation. In Figure 4 we show the  $(x, y)$ -plane density stratification of the region around the head of the bullet flow, and four frames with the stratifications on  $(y, z)$ -cuts, across the flow axis (for a  $t = 50$  yr time integration). The A and B frames cut across the first vortex shed by the bullet flow (see Fig. 4). In these frames, we see that the vortex has a large-scale, approximately circular structure, but that it is broken up into a series of high- and low-density sections (with density contrasts of more than an order of magnitude). Cut C shows that the second vortex shed by the clump has even stronger deviations from axisymmetry. Finally, cut D shows that the leading region of the bow shock has a complex, 3D structure with little vestige of axisymmetry (see Fig. 4).

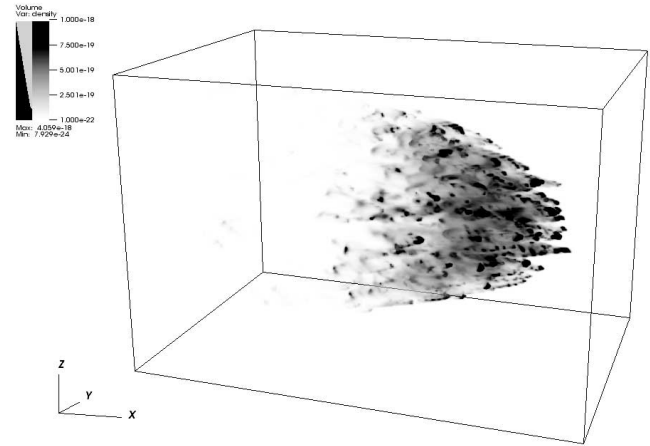


FIG. 6.—Same as Fig. 4, but for the density stratification obtained from the 3D simulation for a  $t = 50$  yr time integration.

The deviations from axisymmetry in the head of the bullet flow can be better appreciated in “volume rendering” representations of the 3D stratification. Figure 5 shows such a representation of the  $t = 10$  yr density stratification. At this time, the cloudlet shock has still not gone through the diameter of the bullet (see Fig. 1 and § 2). The head of the bow shock is already developing a complex structure of dense protrusions.

In the volume rendered,  $t = 50$  yr density stratification (see Fig. 6), we see that the leading region of the flow has developed of order 50 extended, finger-like protrusions. These protrusions have typical lengths of  $\sim 3 \times 10^{15}$  cm and diameters of  $\sim 5 \times 10^{14}$  cm (see Figs. 2 and 5). The diameter of the protrusions is resolved with  $\sim 10$  pixels (see § 2).

#### 4. DISCUSSION

We have carried out an axisymmetric and a 3D numerical simulation of a radiative, “interstellar bullet” flow, with parameters and numerical resolution similar to the ones of the axisymmetric simulation of Poludnenko et al. (2004b). We find that some of the general characteristics of the axisymmetric simulation are still present in the 3D flow.

In both simulations, the head of the bullet flow becomes heavily fragmented (although the details of the fragmentation are different; see below). Also, in both simulations there are “vortex shedding” events, although these are less frequent in the 3D simulation, and in this simulation a strong angular breakup of the vortices also occurs.

The main qualitative difference between the two simulations is that a high-velocity, compact, on-axis condensation is formed at the head of the bullet flow in the axisymmetric simulation. This is one of the more remarkable features of axisymmetric simulations of radiative bullet flows (see Poludnenko et al. 2004b). This axial condensation is absent in our 3D simulation. Actually, the head of the 3D bullet is qualitatively similar to the off-axis regions of the axisymmetric bullet.

We should note that while the bullet is initially homogeneous in the axisymmetric simulation, we have imposed a low-amplitude, 3D sinusoidal density perturbation in the 3D bullet (it is of course impossible to impose the same initial perturbation in the axisymmetric simulation). To some extent, the structure that we obtain in the evolved 3D bullet depends on the nature of this initial perturbation, as can be appreciated from the fact that cross-axis cuts (e.g., of the density stratification of the evolved flow; see Fig. 4) preserve the reflection symmetry on the  $y = z$  axis of the initial sinusoidal

perturbation (see eq. [1]). However, the huge amplitude of the angular fluctuations of the evolved flow (see Figs. 4 and 6) shows that the initial perturbation is indeed feeding true instabilities of the 3D flow.

One could of course start the 3D simulation with an initially homogeneous bullet. Such a simulation does not produce an axisymmetric flow because of the properties of a numerical algorithm applied on a Cartesian division of the cross-flow planes. Therefore, we felt that it is more appropriate to break the axisymmetry by imposing an initial perturbation of known characteristics rather than allowing the deviations from axisymmetry to grow from not well observed, direction-dependent numerical errors.

From our results, we can conclude that even for a low-amplitude initial density perturbation (with maximum deviations of 5% with respect to the mean density; see eq. [1]), large deviations from axisymmetry are obtained in the breakup of the bullet. Therefore, such deviations are also likely to be found in a real, astrophysical bullet flow, in which the initial conditions are likely to have large perturbations from homogeneity.

Another point that we should mention is that the features produced in the head of the evolved bullet flow (see Fig. 6) have diameters of  $\sim 10$  pixels (see the discussion at the end of § 3). This of course raises the suspicion that a breakup into smaller scale features might occur at higher numerical resolutions. Future stud-

ies of 3D bullet flows with resolutions higher by a factor of  $\sim 10$  will be necessary in order to resolve this question.

We end by pointing out that dense axial structures and rings appear in axisymmetric simulations of other flows (for example, of jets), and do not appear in 3D simulations. As far as we are aware, the present work shows the first comparison of axisymmetric and 3D simulations with identical flow parameters and numerical resolution showing the breakup of axisymmetry in bullet flows.

We thank the anonymous referee for the his/her helpful comments. The work of A. R., A. E., and P. V. was supported by the CONACyT grant 46828-F, the DGAPA (UNAM) grant IN 108207 and the “Macroproyecto de Tecnologías para la Universidad de la Información y la Computación” (Secretaría de Desarrollo Institucional de la UNAM, Programa Transdisciplinario en Investigación y Desarrollo para Facultades y Escuelas, Unidad de Apoyo a la Investigación en Facultades y Escuelas). The work of ARi was supported by the Spanish MCyT grants AYA2005-08523-C03-01 and AYA2005-08013-C03-01. We thank Enrique Palacios and Martín Cruz for supporting the servers in which the calculations of this paper were carried out.

#### REFERENCES

- Bouchet, P., Dwek, E., Danziger, J., Arendt, R. G., De Buizer, I. J. M., Sangwook, P., Suntzeff, N. B., Kirshner, R. P., & Challis, P. 2006, *ApJ*, 650, 212
- Corradi, R. L. M., Perinotto, M., Villaver, E., Mampaso, A., & Gonçalves, D. 1999, *ApJ*, 523, 721
- Falle, S. A. E. G., Coker, R. F., Pittard, J. M., Dyson, J. E., & Hartquist, T. W. 2002, *MNRAS*, 329, 670
- Fesen, R. A., et al. 2006, *ApJ*, 645, 283
- Gregori, G., Miniati, F., Ryu, D., & Jones, T. W. 2000, *ApJ*, 543, 775
- Hartigan, P., Raymond, J. C., & Hartmann, L. W. 1987, *ApJ*, 316, 323
- Hartmann, L. W., & Raymond, J. C. 1984, *ApJ*, 276, 560
- Gonçalves, D., Mampaso, A., Corradi, R. L. M., & Perinotto, M. 2004, in *ASP Conf. Ser. 313, Asymmetrical Planetary Nebulae III: Winds, Structure, and the Thunderbird*, ed. M. Meixner, et al. (San Francisco: ASP), 198
- Klein, R. I., Budil, K. S., Perry, T. S., & Bach, D. R. 2003, *ApJ*, 583, 245
- Norman, C., & Silk, J. 1979, *ApJ*, 228, 197
- O’Dell, C. R., Balick, B., Hajian, A. R., Henney, W. J., & Burkert, A. 2002, *AJ*, 123, 3329
- Poludnenko, A. Y., Frank, A., & Mitran, S. 2004a, in *ASP Conf. Ser. 313, Asymmetrical Planetary Nebulae III: Winds, Structure, and the Thunderbird*, ed. M. Meixner et al. (San Francisco: ASP), 434
- . 2004b, *ApJ*, 613, 387
- Raga, A. C., Cantó, J., Curiel, S., & Taylor, S. 1998, *MNRAS*, 295, 738
- Raga, A. C., Mellema, G., Arthur, S. J., Binette, L., Ferruit, P., & Steffen, W. 1999, *Rev. Mex. A&A*, 35, 123
- Raga, A. C., Navarro-González, R., Villagrán-Muniz, M. 2000, *Rev. Mex. A&A*, 36, 67
- Xu, J., & Stone, J. M. 1995, *ApJ*, 454, 172